Skin Permeation: Enhancing Ability of Liquid Crystal Formulations

17

Wesam R. Kadhum, Hiroaki Todo, and Kenji Sugibayashi

Contents

W.R. Kadhum • H. Todo • K. Sugibayashi (✉)
Faculty of Pharmaceutical Sciences, Josai University, 1-1 Keyakidai, Sakado, Saitama 350-0295, Japan
e-mail: rkwesam@josai.ac.jp; ht-todo@josai.ac.jp; sugib@josai.ac.jp

17.1 Introduction

The primary dosage forms used in drug therapy are oral formulations and injections; however, oral formulations have disadvantages, such as the side effect on the gastrointestinal tract and the first-pass effect, while injections cause pain by needle puncture and may cause infection; transdermal drug delivery systems (TDDS) can avoid these disadvantages. Interestingly, more TDDS were developed at the beginning of this century than oral DDS. The outermost layer of the skin, the stratum corneum (SC), has a role as the primary barrier against water evaporation from the body and skin permeation of most drugs into the body. Thus, overcoming the SC barrier is important to advance the development of TDDS.

Chemical approaches, such as penetration enhancers (Purdon et al. 2004), and physical approaches, such as iontophoresis (Banga and Kasha 2008), phonophoresis (Ogura et al. 2008), and electroporation (Tokudome and Sugibayashi 2004; Tokumoto et al. 2005), have been evaluated to increase the skin permeation of several drugs. Formulation approaches have also been investigated to increase the skin permeation of drugs. Liposomes and niosomes are examples for new topical formulations having high penetration-enhancing activity of the entrapped drugs (Abraham and Downing 1989; Fang et al. 2001; Kirjavainen et al. 1999); in general, however, such nano-sized materials have poor stability.

N. Dragicevic, H.I. Maibach (eds.), *Percutaneous Penetration Enhancers Chemical Methods in Penetration Enhancement: Drug Manipulation Strategies and Vehicle Effects*,
DOI 10.1007/978-3-662-45013-0_17, © Springer-Verlag Berlin Heidelberg 2015

Recently, solid lipid nanoparticles (Dingler and Gohla 2002; Müller et al. 2000) and liquid crystal (LC) dispersions have been developed for topical formulations, and the latter is highly bioadhesive (Geraghty et al. 1997) and physically stable. The LC structure is very similar to the intracellular lipid structure in the SC (Norlén 2001). Very stable LC dispersions made of monoolein/oleic acid (Garg et al. 2007; Gustafsson et al. 1996) and phytol (Barauskas and Landh 2003) have been applied to the skin and mucosa. LC nanodispersions containing monoolein/oleic acid were used to modify the skin permeation of indomethacin (Esposito et al. 2005), cyclosporine (Lopes et al. 2006a, b), vitamin K (Lopes et al. 2007), and propranolol (Namdeo and Jain 2002). These LCs have also been investigated for skin care products (Brinon et al. 1999; Esposito et al. 2007) and cubic lipid structures have already been used as lotions and creams in cosmetics (Yamaguchi et al. 2006).

17.2 Liquid Crystals (LC)

LCs are self-assembled mesophases, which are intermediates between isotropic liquids and crystalline solids (Gin et al. 2008b). In LC phases, long-range periodicity exists, although the molecules exhibit a dynamical disorder at atomic distances, as is the case of liquids. Therefore, these materials can also be considered ordered fluids (Larsson 1989). On the other hand, lyotropic LCs are materials that are composed from at least two molecules: an amphiphilic molecule and its solvent. A hydrophilic solvent, such as water, hydrates the polar moieties of the amphiphiles via hydrogen bonding, while the flexible aliphatic tails of the amphiphiles aggregate into fused hydrophobic regions, based on van der Waals interactions between aliphatic lipids and hydrophobic regions. In addition to morphologic dependence on the chemical composition, lyotropic LCs are also sensitive to external parameters, such as temperature and pressure (Gin et al. 2008b; Larsson 1989; Yuli-Amar 2008). Therefore, the shape of the amphiphilic molecule, critical packing parameters, and interfacial curvature energy are important parameters for the structure and nature of LCs (Silver 1985).

An important feature of lyotropics is the self-assembly of the amphiphilic molecules as supermolecular structures, which are the basic units of these mesophases.

The major LC structures are lamella, hexagonal, reverse hexagonal, bicontinuous cubic, and micellar cubic. Among them, hexagonal liquid crystals, reverse-hexagonal liquid crystals, and cubic liquid crystals are known as non-lamella liquid crystals (non-lamella LC).

Hexagonal liquid crystal and reverse-hexagonal liquid crystals are formed by some amphiphilic molecules when they are mixed with water or another polar solvent. In this phase, the amphiphilic molecules are aggregated into cylindrical structures of indefinite length and these cylindrical aggregates are disposed on a hexagonal lattice, giving the phase long-range orientational order (Scheme 17.1).

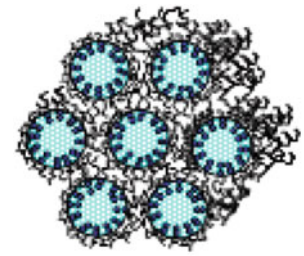

Scheme 17.1 A schematic representation of hexagonal phase

Whereas cubic liquid crystals are formed when the concentration of micelles dispersed in a solvent is sufficiently high that they are forced to pack into a structure having long-ranged positional order (Scheme 17.2).

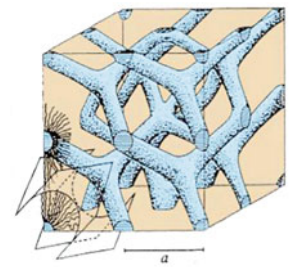

Scheme 17.2 A schematic representation of cubic phase

On the other hand, liposomes as lamella LC have an entrapped, discontinuous aqueous phase separated by bilayered lamellae from the continuous aqueous phase (Scheme 17.3).

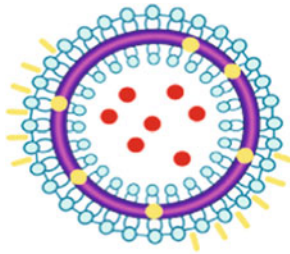

Scheme 17.3 A schematic representation of a liposome

Thus, the evaluation of lamella LC as a drug carrier might be difficult because entrapped drug could easily transfer from the internal phase to the dispersion medium.

17.3 Current Problems in LC for TDDS

Phytantriol and glyceryl monooleate (GMO) are well-known compounds as non-lamella LC-forming lipoids (Phan et al. 2011). However, not all of drugs can be entrapped in non-lamella LC because hydrophilic/lipophilic balance (HLB) and molecular size of drugs (Charlotte and Drummond 2013) might affect the self-assemble of non-lamella LC-forming lipids. Furthermore, conventional non-lamella LC-forming lipids have so high viscosity that it would be tough to handle them in drug and cosmetic formulations and these lipids can form non-lamella LC in a narrow temperature range. These are problems that need to be overcome for the development of transdermal formulations using non-lamella LCs.

17.4 Structure of Liquid Crystal Dispersion

Figure 17.1 illustrates a scheme of the formation of lamella LC and non-lamella LC from amphiphiles in water (Gin et al. 2008a). Lamellar, hexagonal, bicontinuous cubic, and discontinuous cubic phases are well known and there are many research studies in that field. The structure of self-assembled mesophases is affected by amphiphile's concentration. On increasing the concentration of amphiphiles in water, liposomes (lamellar), bicontinuous cubic lamella phases (Q2), and hexagonal phases (H2) are formed. There have been numerous descriptions of the liquid crystalline phase behavior (Hyde 1990). The dimensionless shape parameter known as critical packing parameter (CPP) has provided useful information regarding the choice of type of rational design of amphiphile-water phase behavior (e.g., micelle structure is when CPP <1, lamellar phase is when CPP=1, and inverse cubic structure is when CPP> 1) (Israelachvili 1976). In this chapter, we focus on cubic lamella phase and hexagonal phase that show skin permeation enhancement effects.

17.5 Preparation of a Mixture of Mono-, Di-, and Triesters (1) and Monoesters (2) Composed of Erythritol and Phytanylacetic Acid

Erythritol (2.50 kg) was dissolved in dimethyl sulfoxide (10.8 kg) at 100 °C under nitrogen purging, before the addition of anhydrous calcium carbonate (37.8 g) at 80 °C. Methyl phytanylacetate (5,9,13,17-tetramethyloctadecanoate) (4.83 kg) was added dropwise to the solution under reduced pressure over 2.5 h. The reaction mixture was refluxed under reduced pressure overnight, while the methanol produced was gradually distilled. After cooling, the mixture was neutralized by the addition of formic acid (29 g) and concentrated in vacuo. The residue (6.1 kg) was diluted with t-butyl methyl ether (18.3 kg) and filtered to remove the remaining erythritol. The filtrate was diluted again with t-butyl methyl ether (24 kg), washed twice with aqueous sodium bicarbonate, and concentrated in vacuo at 100 °C. The product obtained (4.7 kg, mixture 1) consisted of

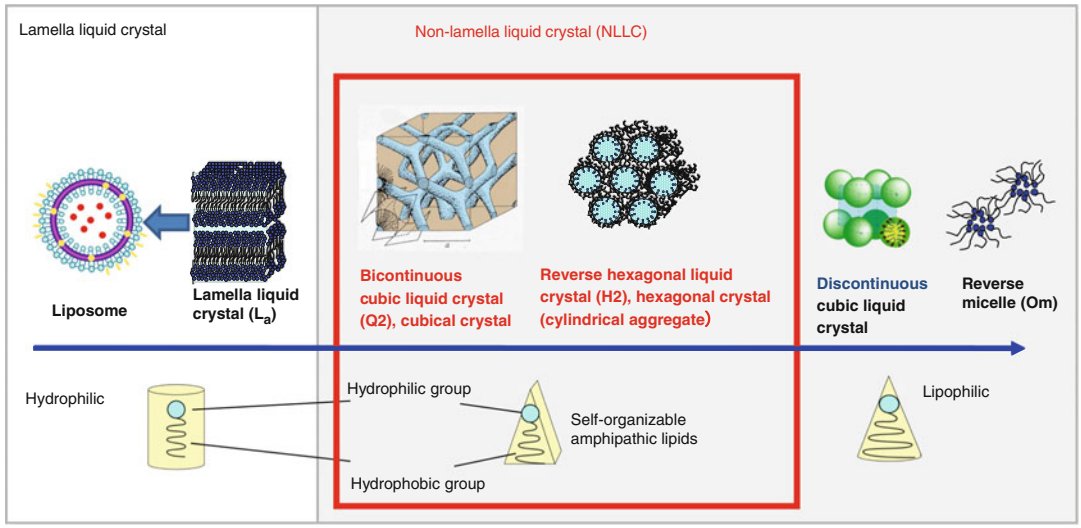

Fig. 17.1 Change of self-assembled structure of LC and non-lamella LC-forming lipids. The states of self-assembled structure depend on balance of polar/nonpolar groups (CPP value) and existence of salt or pH values in water phases. The *arrow* shows transitions of liquid crystals regarding lipophilicity of solvent

Table 17.1 Composition of liquid crystal dispersions

Ingredients	30 mM calcein-entrapped LC-A (%)	Blank (%)
1-o-(5,9,13,17-tetramethyloctadecanoyl) erythritol (crude, 1)	10.0	10.0
Sodium calcein	2.0	–
Pluronic® F127 (10 %)	10.0	10.0
Methyl *p*-hydroxybenzoate	0.1	0.1
Purified water	77.9	79.9
Total	100	100.0
Ingredients	30 mM calcein-entrapped LC-B (%)	Blank (%)
1-o-(5,9,13,17-tetramethyloctadecanoyl) erythritol (pure, 2)	10.0	10.0
Calcein (sodium)	0.2	–
Pluronic® F127 (20 %)	10.0	10.0
Methyl *p*-hydroxybenzoate	0.1	0.1
Purified water	79.7	79.9
Total	100	100.0

monoesters (36 %), diesters (12 %), and triesters (52 %) of erythritol and phytanylacetic acid (the ratio was determined by gas chromatography analysis). Mixture 1 was purified by column chromatography using silica gel (Wakogel C-300, Wako Pure Chemicals Industries, Ltd., Osaka, Japan) to afford monoesters 2 of 1-O- and 2-O-phytanylacetyl-erythritol.

17.6 Preparation of Liquid Crystal Dispersion

Table 17.1 shows the composition of liquid crystal A (LC-A) and liquid crystal B (LC-B) nanodispersions. Ten grams of crude ester 1 or pure ester 2 was used to prepare LC-A and LC-B, respectively. In this step, LC-A and LC-B were

semisolid and were nano-dispersed using a high-pressure emulsifier (NM2-L200AR, Yoshida Kikai Co., Ltd, Nagoya, Japan) or an ultrasonic homogenizer (USP-50, Shimadzu Corp., Kyoto, Japan), respectively, in aqueous solution (90.0 g) containing sodium calcein, Pluronic® F127 and methyl p-hydroxybenzoate. Calcein concentrations in LC-A and LC-B were different (see Table 17.1).

17.7 Structure of Liquid Crystal Dispersions Observed by Cryo-TEM Microscope

Skin permeation enhancement effects of non-lamella LCs, which consist of crude or pure non-lamella LC-forming lipids, such as 1-O-(5,9,13,17-tetramethyloctadecanoyl) erythritol (Fig. 17.2), are discussed in this chapter. The crude and pure esters were used to prepare non-lamella LC-A and non-lamella LC-B, respectively. Non-lamella LC-A- and non-lamella LC-B-forming lipids were dispersed in aqueous solution containing sodium calcein to prepare non-lamella LCs. Sodium calcein (*M.W.*; 623) is a good indicator used as hydrophilic fluorescent marker for skin permeation experiment. Thus, penetration-enhancing ability of non-lamella LC was investigated by evaluating the permeation of calcein through skin.

Figure 17.3 shows cryo-transmission electron microscope (TEM) micrographs of non-lamella LC-A and non-lamella LC-B. Similar to the cryo-TEM micrographs of cubic non-lamella LC prepared by monoolein and oleic acid (Garg et al. 2007; Gustafsson et al. 1996), non-lamella LC structures were observed in non-lamella LC-A and non-lamella LC-B (in white circles in

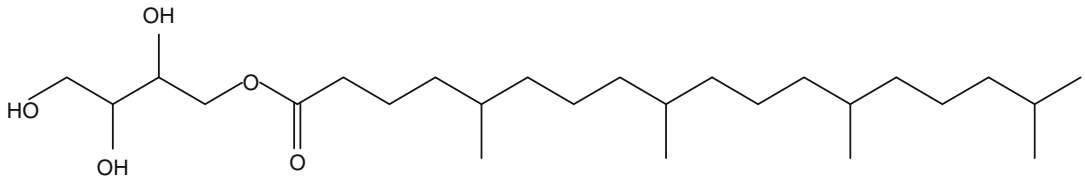

Fig. 17.2 Chemical structure of 1-o-(5, 9, 13, 17-tetramethyloctadecanoyl) erythritol

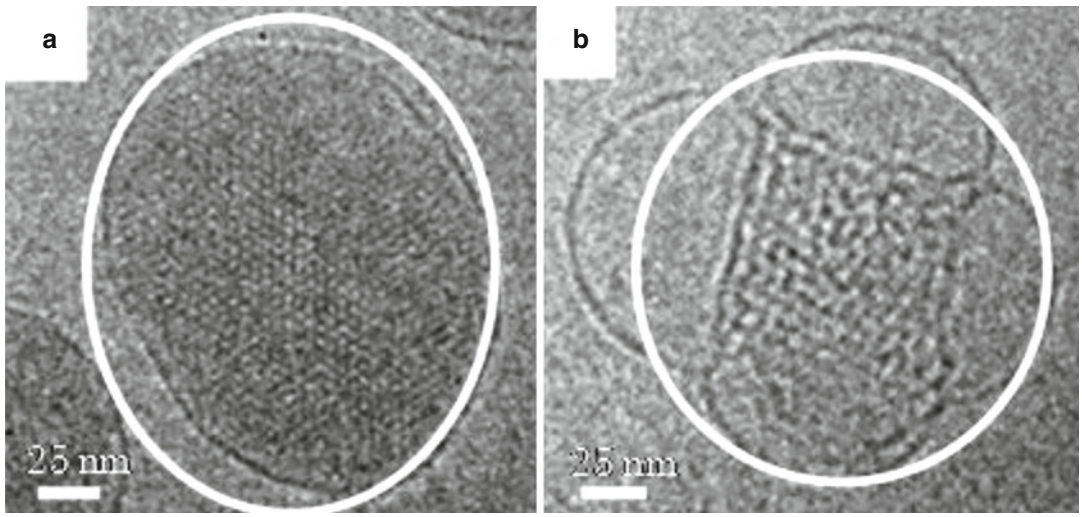

Fig. 17.3 Cryo-TEM microscope images of liquid crystal dispersions. Images (**a**, **b**) are non-lamella LC-A and non-lamella LC-B, respectively. Non-lamella LC structures were found in both (**a**, **b**) (see *circles* in images). Each *white bar* indicates 25 nm length

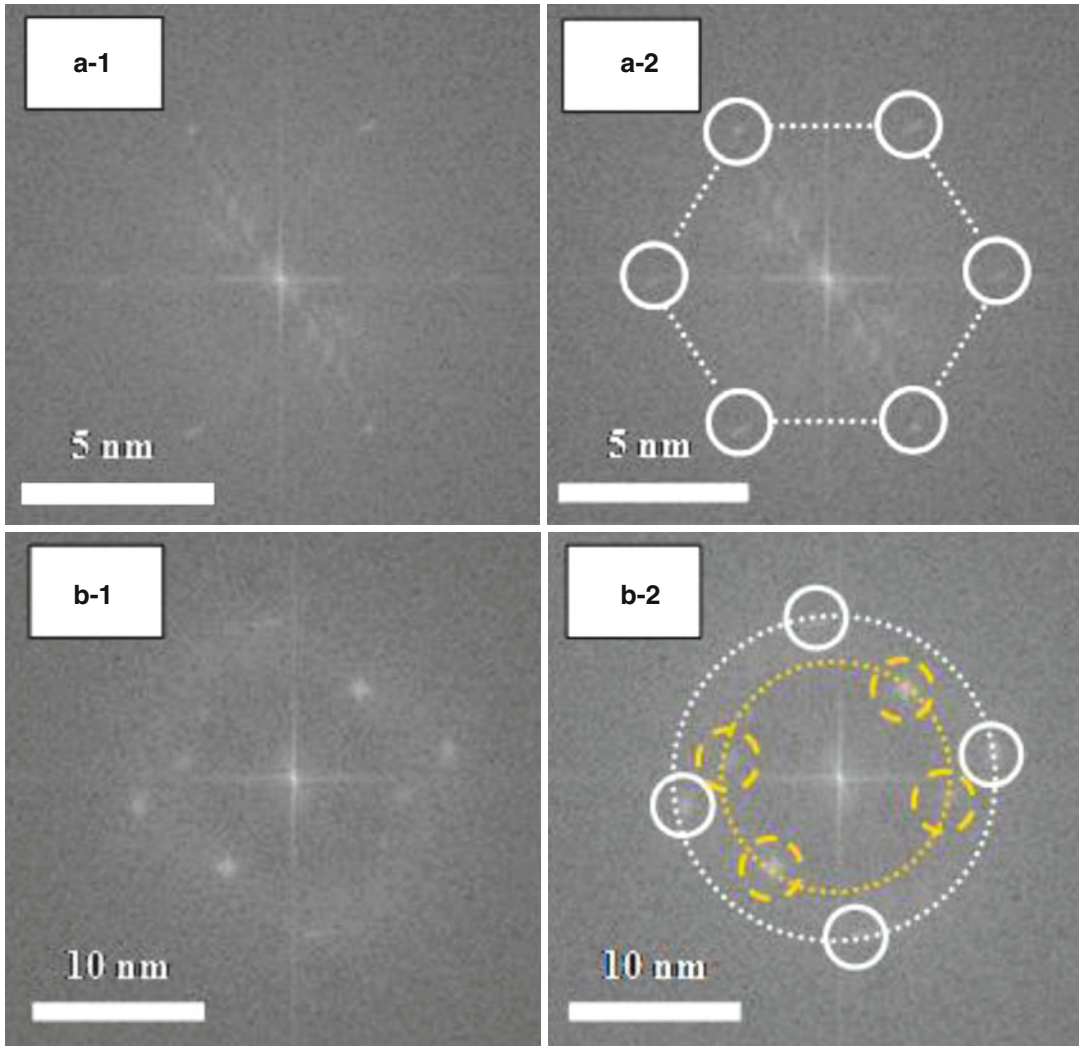

Fig. 17.4 Electron diffraction pattern of liquid crystal dispersions. (**a**-1) and (**a**-2) and (**b**-1) and (**b**-2) show the same images of LC-A and LC-B, respectively, without and with auxiliary lines and marks. (**a**-2) shows hexagonal LC, having 4.6 nm periodic structure. (**b**-2) illustrates cubic LC, having two periodic structures of 6.0 and 9.0 nm cycles. *White bars* indicate 5 or 10 nm length

Fig. 17.3). Figure 17.4 shows electronic diffraction patterns of non-lamella LC determined by cryo-TEM photographs. It was found from these diffraction patterns that non-lamella LC-A was a hexagonal non-lamella LC, having 4.6 nm periodic structure (A-2 dashed lines in Fig. 17.4), and non-lamella LC-B was a cubic non-lamella LC, having two periodic structures of 6.0 and 9.0 nm (B-2 dashed lines in Fig. 17.4).

17.8 Skin Penetration-Enhancing Effect of Liquid Crystals

The penetration-enhancing effectiveness of non-lamella LC in topical formulations was evaluated by measuring permeation of a mal-absorbable compound, calcein, through excised hairless rat skin and through the three-dimensional cultured human skin model (LSE-high).

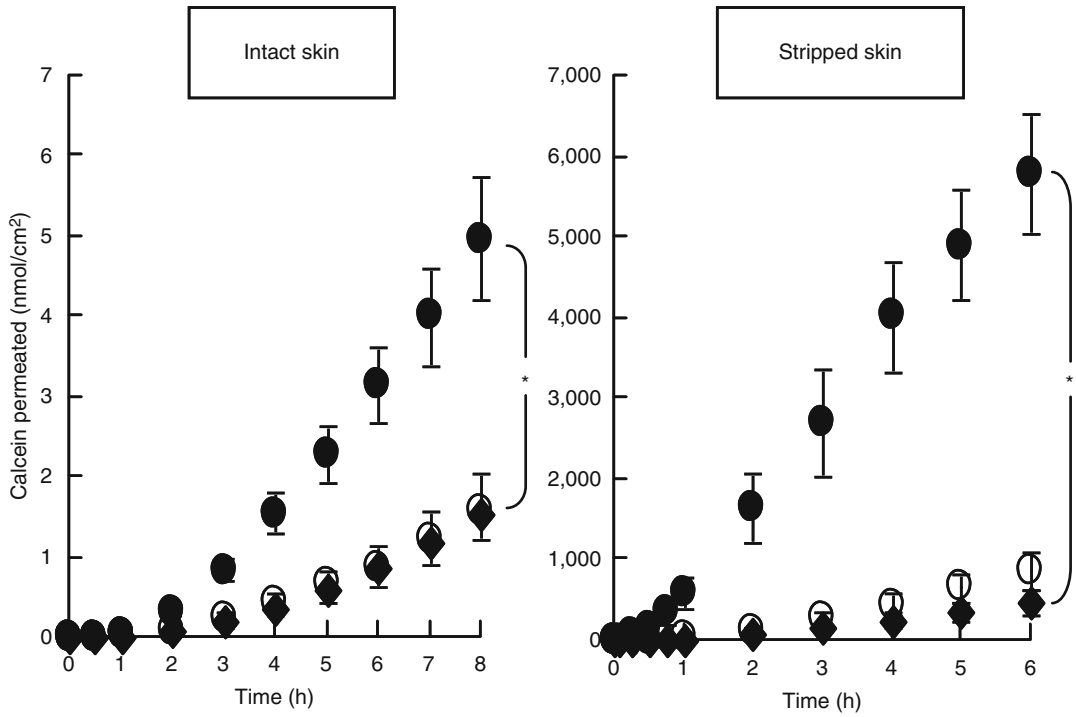

Fig. 17.5 Effect of non-lamella LC-A formulation on the time course of the cumulative amount of calcein that permeated intact and stripped hairless rat skin. Symbols are as follows: ◆ free calcein, ○ free calcein plus non-lamella LC-A, ● calcein entrapped in non-lamella LC-A. *Asterisks* mean significant difference between calcein entrapped in non-lamella LC-A and free calcein or free calcein plus non-lamella LC-A (p <0.05). Each point represents the mean ± S.E. of at least three to seven experiments

Figure 17.5 shows the time course of calcein permeation through excised hairless rat skin from the reverse-hexagonal liquid crystal (non-lamella LC-A) formulations. In both intact and stripped skin, the skin permeations of calcein from calcein entrapped in non-lamella LC-A formulation provided a 3 and 10 times higher, respectively, than the permeation of calcein from free calcein solution. In addition, the mixture of blank non-lamella LC-A dispersion and free calcein showed similar skin permeation to that of free calcein solution. Thus, the blank non-lamella LC formulation itself did not show any penetration-enhancing effect. Permeation parameters were determined from the time course of the cumulative amount of the permeated drug. The calculated parameters are shown in Table 17.2. Partition coefficient, K, of calcein was markedly increased by application of the calcein entrapped in non-lamella LC-A formulation, suggesting that non-lamella LC-A could improve the calcein distribution into the skin by providing a high affinity to intercellular lipid structure in the skin (stratum corneum). Next, the time course of the skin permeation of calcein from the cubic liquid crystal dispersion (non-lamella LC-B) was evaluated; the results are shown in Fig. 17.6. Non-lamella LC-B as well as non-lamella LC-A enhanced the permeation of calcein through intact hairless rat skin; Table 17.3 summarizes the permeation parameters for non-lamella LC-B. Increased partition of calcein was observed by non-lamella LC-B, as by non-lamella LC-A. In contrast, no increase in drug partition was observed in stripped skin from non-lamella LC-B or from non-lamella LC-A. Non-lamella LC-A has a high affinity for the stratum corneum as well as the viable epidermis, whereas non-lamella LC-B shows high affinity for the stratum corneum, but not for the viable epidermis.

Table 17.2 Partition coefficient (K), diffusion coefficient (D), and permeability coefficient (P) of calcein through hairless rat skin after application of different formulations of non-lamella LC-A

	30 mM calcein	Calcein entrapped in non-lamella LC-A	Free calcein and non-lamella LC-A
Intact skin			
K	0.10 ± 0.02	0.22 ± 0.04	0.09 ± 0.03
D ($\times 10^{-11}$ cm^2/s)	6.05 ± 0.52	7.54 ± 0.18	6.75 ± 0.68
P ($\times 10^{-9}$ cm/s)	2.91 ± 0.55	8.32 ± 1.33	2.80 ± 0.91
Stripped skin			
K	0.52 ± 0.13	2.51 ± 0.87	1.19 ± 0.20
D ($\times 10^{-7}$ cm^2/s)	1.04 ± 0.07	3.22 ± 1.14	0.89 ± 0.07
P ($\times 10^{-7}$ cm/s)	9.41 ± 2.86	110 ± 12.5	18.9 ± 4.51

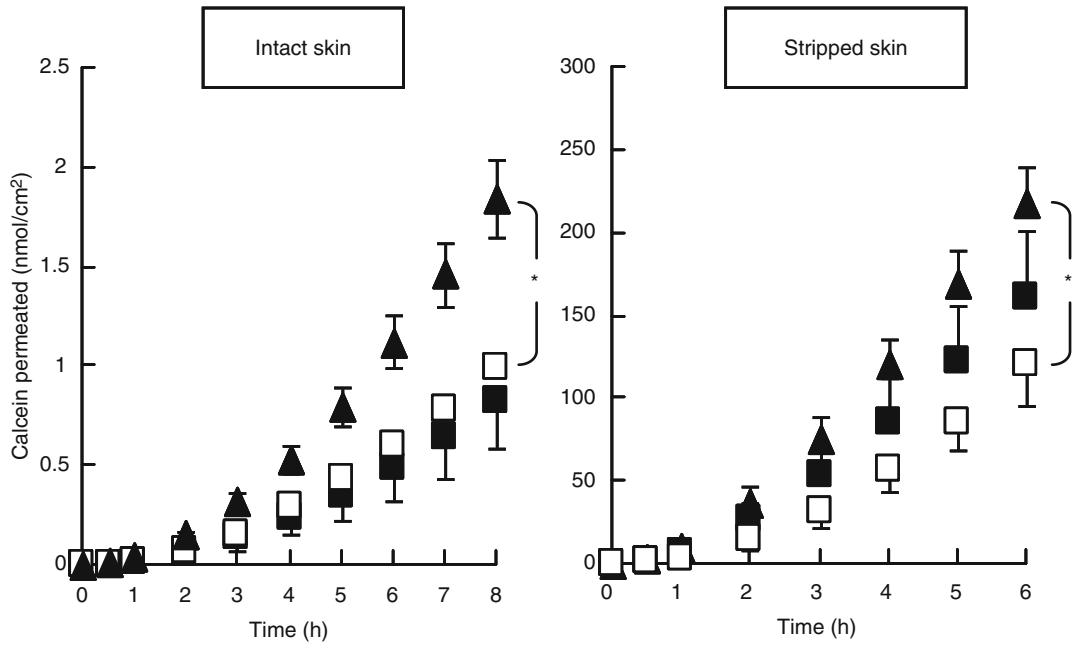

Fig. 17.6 Effect of LC-B formulation on the time course of the cumulative amount of calcein that permeated through intact and stripped hairless rat skin. Symbols are as follows: ■ free calcein, □ free calcein plus non-lamella LC-B, ▲ calcein entrapped in non-lamella LC-B. Asterisks mean significant difference between calcein entrapped in LC-A and free calcein or free calcein plus non-lamella LC-B (p <0.05). Each point represents the mean ± S.E. of at least 3–12 experiments

Table 17.3 Partition coefficient (K), diffusion coefficient (D), and permeability coefficient (P) of calcein through hairless rat skin after application of different formulations of non-lamella LC-B

	3 mM calcein	3 mM calcein in 2 % Pluronic sol.	Free calcein and non-lamella LC-B
Intact skin			
K	0.53 ± 0.12	0.59 ± 0.11	0.95 ± 0.10
D ($\times 10^{-11}$ cm^2/s)	5.95 ± 0.78	6.47 ± 0.74	6.94 ± 0. 39
P ($\times 10^{-8}$ cm/s)	1.56 ± 0.38	1.84 ± 0.13	3.23 ± 0.32
Stripped skin			
K	2.18 ± 0.08	2.44 ± 0.39	2.53 ± 0.26
D ($\times 10^{-8}$ cm^2/s)	9.04 ± 1.33	6.92 ± 2.83	10.7 ± 1.45
P ($\times 10^{-6}$ cm/s)	3.46 ± 0.65	2.95 ± 0.55	4.48 ± 0.32

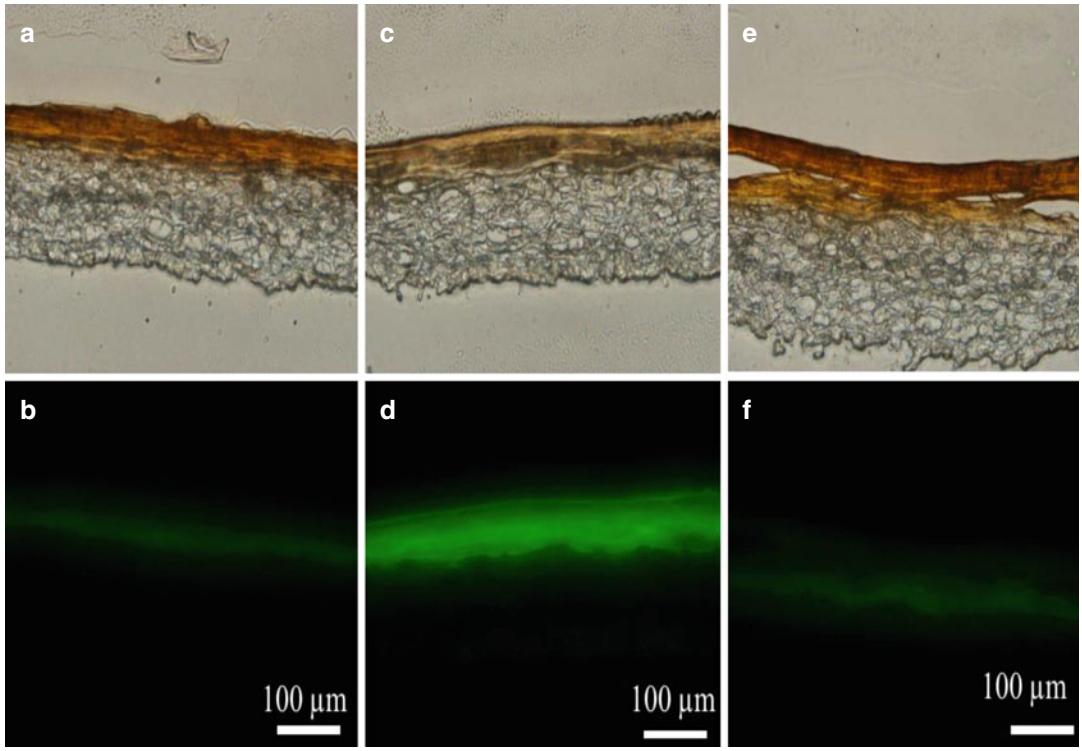

Fig. 17.7 Histological observation of LSE-high, 8 h after application of non-lamella LC-A dispersion with entrapped calcein. Images (**a**, **b**) are for free calcein, (**c**, **d**) for calcein entrapped in non-lamella LC-A dispersion, and (**e**, **f**) for physical mixture of free calcein and non-lamella LC-A dispersion. Images (**a**, **c**, **e**) show light micrograph images and (**b**, **d**, **f**) show corresponding fluorescent images. Bars indicate 100 mm (*vertical slice*)

17.9 Drug Distribution in Skin After Topically Applied Non-lamella LCs

Similar permeation experiments were carried out using a three-dimensional cultured human skin model (LSE-high). Since no appendages, such as hair follicles and sweat ducts, are present in LSE-high, the penetration-enhancing effect by non-lamella LC formulations must be due to the enhanced drug penetration through the stratum corneum barrier, i.e., through the intercellular route. Figures 17.7a–f show the cross section of LSE-high, 8 h after application of free calcein and calcein entrapped in non-lamella LC-A and simultaneous application of free calcein and non-lamella LC-A, respectively. Figures 17.7a, c, and e show hematoxylin and eosin (HE)-stained micrographs and Fig. 17.7b, d, and f show corresponding fluorescent micrographs. Similar fluorescent level was observed for groups of free calcein (Fig. 17.7b) and free calcein plus non-lamella LC-A dispersion (Fig. 17.7f). In contrast, a much higher fluorescent level was found for the calcein entrapped in non-lamella LC-A (Fig. 17.7d). These results were also obtained by the skin permeation study using non-lamella LC-A dispersion with entrapped or free calcein and the calcein solution (Fig. 17.5).

Conclusion

It was found from cryo-TEM observation and electron diffraction pattern analysis that these LC-A and LC-B nano-dispersions have reverse-hexagonal LC and cubic LC dispersions, respectively. These LC dispersions were very stable, since no aggregation (diameter growth) was observed. The entrapping ratio of a hydrophilic model compound, calcein, in LC-B was higher than in LC-A, suggesting that cubic LC has great entrapping potency for hydrophilic materials. Other drugs with different lipophilicity and molecular weights must

be determined in the future. The present skin permeation experiments showed that LC-A and LC-B nano-dispersions increased the skin permeation of the entrapped drug, probably due to increased partition of the LC in the skin barrier. Thus, the presently prepared LC formulations can be utilized as new topical formulations for therapeutic drugs and cosmetic ingredients, especially for hydrophilic compounds. The skin content of the entrapped drugs and detail mechanistic analysis must be determined in the near future.

References

Abraham W, Downing DT (1989) Preparation of model membranes for skin permeability studies using stratum corneum lipids. J Invest Dermatol 93:809–813

Barauskas J, Landh T (2003) Phase behavior of phytantriol/water system. Langmuir 19:9562–9565

Brinon L, Geiger S, Alard V, Doucet J, Tranchant JF, Couarraze G (1999) Percutaneous absorption of sunscreens from liquid crystalline phases. J Control Release 60:67–76

Conn CE, Drummond CJ (2013) Nanostructured bicontinuous cubic lipid self-assembly materials as matrices for protein encapsulation. Soft Matter. doi:10.1039/C3SM27743G

Dingler A, Gohla S (2002) Production of solid lipid nanoparticles (SLN): scaling up feasibilities. J Microencapsul 19:11–18

Esposito E, Cortesi R, Drechsler M, Paccamiccio L, Mariani P, Contado C, Stellin E, Menegatti E, Bonina F, Puglia C (2005) Cubosome dispersions as delivery systems for percutaneous administration of indomethacin. Pharm Res 22:2163–2173

Esposito E, Drechsler M, Mariani P, Sivieri E, Bozzini R, Montesi L, Menegatti E, Cortesi R (2007) Nanosystem for skin hydration: a comparative study. Int J Cosmet Sci 29:39–47

Fang J, Hong C, Chiu W, Wang Y (2001) Effect of liposomes and niosomes on skin permeation of enoxacin. Int J Pharm 219:61–72

Geraghty PB, Attwood D, Collett JH, Sharma H, Dandiker Y (1997) An investigation of the parameters influencing the bioadhesive properties of Myverol 18–99/water gels. Biomaterials 18:63–67

Gin DL, Pecinovsky CS, Bara JE, Kerr RL (2008a) Functional lyotropic liquid crystal materials. Liquid crystalline functional assemblies and their supramolecular structures and bonding. 128:181–222

Gin DL, Pecinovsky CS, Bara JE, Kerr L (2008b) Functional lyotropic liquid crystal materials. Struct Bond 128:181

Garg G, Saraf S, Saraf S (2007) Cubosomes, an overview. Biol Pharm Bull 30:350–353

Gustafsson J, Ljusberg-Wahren H, Almgren M, Larsson K (1996) Cubic lipid-water phase dispersed into submicron particles. Langumuir 12:4611–4613

Hyde ST (1990) Curvature and the global structure of interfaces in surfactant-water systems. J Phys Colloq 51(C7):209–228

Israelachvili JN, Mitchel DJ, Ninham BW (1976) Theory of self-assembly of hydrocarbons amphiphiles into micelles and bilayers. J Chem Soc Faraday Trans 2(72):1525–1568

Kasha PC, Banga AK (2008) A review of patent literature for iontophoretic delivery and devices. Recent Pat Drug Deliv Formul 2:41–50

Kirjavainen M, Urtti A, Valjakka-Koskelab R, Kiesvaara J, Mönkkönena J (1999) Liposome–skin interactions and their effects on the skin permeation of drugs. Eur J Pharm Sci 7:279–286

Larsson K (1989) Cubic lipid-water phases: structure and biomembrane aspects. J Phys Chem 93:7304–7314

Lopes LB, Ferreira DA, de Paula D, Garcia MTJ, Thomazini JA, Fantini MCA, Bentley MVLB (2006a) Reverse hexagonal phase nanodispersion of monoolein and oleic acid for topical delivery of peptides: in vitro and in vivo skin penetration of cyclosporin A. Pharm Res 23:1332–1342

Lopes LB, Lopes JLC, Oliveira DCR, Thomazini JA, Garcia MTJ, Fantini MCA, Collett JH, Bentley MVLB (2006b) Liquid crystalline phases of monoolein and water for topical delivery of cyclosporin A, characterization and study of in vitro and in vivo delivery. Eur J Pharm Biopharm 63:146–155

Lopes LB, Speretta FFF, Bentley MVLB (2007) Enhancement of skin penetration of vitamin K using monoolein-based liquid crystalline systems. Eur J Pharm Sci 32:209–215

Müller RH, Mäder K, Gohla S (2000) Solid lipid nanoparticles (SLN) for controlled delivery – a review of the state of the art. Eur J Pharm Biopharm 50:161–177

Namdeo A, Jain NK (2002) Liquid crystalline pharmacogel based enhanced transdermal delivery of propranolol hydrochloride. J Control Release 82:223–236

Norlén L (2001) Skin barrier formation, the membrane folding model. J Invest Dermatol 117:823–829

Ogura M, Paliwal S, Mitragotri S (2008) Low-frequency sonophoresis: current status and future prospects. Adv Drug Deliv Rev 60:1218–1223

Phan S, Fong WK, Kirby N, Hanley T, Boyd BJ (2011) Evaluating the link between self-assembled mesophase structure and drug release. Int J Pharm 421:176–182

Purdon CH, Azzi CG, Zhang J, Smith EW, Maibach HI (2004) Penetration enhancement of transdermal delivery–current permutations and limitations. Crit Rev Ther Drug Carrier Syst 21:97–132

Silver B (1985) The physical chemistry of membranes. Solomon Press, Winchester

Tokudome Y, Sugibayashi K (2004) Mechanism of the synergic effects of calcium chloride and electroporation on the in vitro enhanced skin permeation of drugs. J Control Release 95:267–274

Tokumoto S, Mori K, Higo N, Sugibayashi K (2005) Effect of electroporation on the electroosmosis across hairless mouse skin in vitro. J Control Release 105:296–304

Yamaguchi Y, Nakamura N, Nagasawa T, Kitagawa A, Matsumoto K, Soma Y, Matsuda T, Mizoguchi M, Igarashi R (2006) Enhanced skin regeneration by nanoegg formulation of all-trans retinoic acid. Pharmazie 61:117–121

Yuli-Amar I (2008) Ph.D. Dissertation, The Hebrew University of Jerusalem